Hydromagnetic Flow of Casson Fluid Over a Stretching Plane Through Porous Medium

Deepak K. Maurya[1,a], **Satya Deo**[2,b] **and Pankaj Kumar Maurya**[2,c]

[1]Department of Mathematics, V. B. S. Purvanchal University, Jaunpur, 222003 (U.P.) India

[2]Department of Mathematics, University of Allahabad, Prayagraj, 211002 (U.P.) India

Abstract

The current analysis focuses on the MHD effects of a steady Casson fluid flowing over a stretching sheet in the porous medium. To examine the properties of non-Newtonian fluid, a mathematical model for Casson fluid is developed. Similarity transformation is used to convert higher order nonlinear governing partial differential equations (PDEs) into ordinary differential equations (ODEs). Analytical expressions of flow characteristics like velocity and skin friction coefficient are produced by applying the proper boundary conditions. Reports on specific instances of skin friction coefficient and fluid velocity (horizontal/transversal) are supplied. For various values of flow parameters, such as Casson parameter, suction velocity, conductivity, and permeability parameter, fluid flow characteristics, *i.e.* velocity profiles, and skin friction coefficient are sketched and analysed.

MSC (2020): 76A05, 76S05, 76W05, 35C05

Keywords: Porous media, Casson fluid, suction velocity, non-linear dynamics, similarity transformation

1 Introduction

Casson fluid is identified by two flow parameters in which one parameter is yield stress, which is connected with the attractive force between fluid particles and while the other parameter is plastic viscosity, which relates with asymmetry of the fluid particles [1]. Micropolar liquids [2] are the fluids having microstructure and couple stress effect, clas-

[a]deepak893395@gmail.com (corresponding author)

[b]satyadeo@allduniv.ac.in

[c]pkmaurya_maths@allduniv.ac.in

sified as fluids with non-symmetric stresses [3]. The analytical solution corresponding to the viscous fluid flow at the stagnation point on a vertical plane, studied by Rott [4]. Connection between dimensional analysis and the similarity is explained in the book [5]. Similarity solution for the fluid flow characteristics with uniform suction velocity at the smooth wall is obtained [6]. Vajravelu and Rollins [7] studied the heat transfer characteristics in a conducting fluid over a plane. Effects of chemical reaction [8] on convective heat and mass transfer over a porous stretching surface. Aurthur *et al.* [9] reported the flow of Casson fluid over a porous surface in the presence of uniform magnetic field. Incompressible viscous MHD nanofluid flowing over non-linear stretching surface, is investigated [10].

Krishna *et al.* [11] reported convection flow of a incompressible, viscous and heat-absorbing fluid through a porous medium over a flat plate. Krishna and Chamkha [12] reported the hall and ion slip effects on MHD rotating flow of nanofluids past a semi-infinite permeable moving plate using the perturbation technique. Stagnation point [13] flow of a Casson fluid over a nonlinear stretching sheet with the viscous dissipation, is studied. Flow of the Casson fluid past a permeable stretching plane is discussed [14]. Akbar *et al.* [15] investigated a mathematical model for fluid flow, mass and heat transfer of a Casson fluid to study the non-Newtonian behavior of the flowing fluid. Effects of thermal radiation on mixed convective boundary layer flow from a vertical porous stretching surface in presence of slip embedded in porous medium, reported by Mukhopadhyay [16, 17]. The unsteady flow of a non-Newtonian fluid over a stretching surface is investigated [18].

The governing equation for fluid flow through the porous medium given by a modification of Darcy's equation [19]. Stream function solution of the Brinkman equation in the cylindrical (circular/parabolic) coordinates is obtained [20, 21]. Using cell models, influence of magnetic field on hydrodynamic permeability of biporous membrane relative to the micropolar fluid motion, investigated by Deo *et al.* [22, 23]. Tiwari and Deo [24] studied the pulsatile flow of the Newtonian fluid in flowing through a tube with a permeable wall. Maurya *et al.* [25] presented a comparative study of stream lines, velocities and microrotations for flow of micropolar fluid happening through a porous circular tube for different BVPs. Deo and Maurya [26] reported the drag for flow of micropolar liquid

through a porous cylinder which is embedded in another infinite porous medium. Recently, Maurya and Deo [27] discussed the graphical behaviours of volumetric flow rate and fluid velocity for the problem of MHD effects on Newtonian fluid which is sandwiched between two coaxial porous pipes which are filled with non-Newtonian liquids. Recently, Deo and Maurya [32] studied the MHD effects on the flow of a Newtonian fluid sandwiched between two immiscible micropolar fluid layers through a porous channel. For fractional linear/non-linear two-dimensional partial differential equations, a class of boundary value challenges is investigated by Jaiswal *et al.* [33].

2 Mathematical formulation

Consider the two dimensional laminar boundary layer flow of an incompressible, electrically conducting Casson fluid (*i.e.* non-Newtonian) over a steady stretching sheet ($y = 0$). Two equal and opposite forces F are applied along the $x-$axis (measured tangential to the sheet) and an uniform magnetic field M is imposed along $y-$axis to make the origin fixed, whenever the virtual vertical wall is stretched. The fluid motion is compelled to flow over the upper half plane (*i.e.* $y \geq 0$) and the coordinate axes x and y are considered in tangential and normal directions to the chosen porous stretchable sheet. The geometrical view of present fluid flow problem of density ρ is displayed in the figure 1. The fluid velocity components u and v are the velocities in the directions of x and y axes, respectively.

Assuming that T_{ij}, e_{ij}, μ_P, and p_y are the stress tensor, $(i,j)^{th}$ component of strain-rate tensor, plastic dynamic viscosity coefficient and yield stress of the Casson fluid, respectively. Mathematical symbol Π_c is the critical value of Π with $\Pi = e_{ij}e_{ij}$. The constitutive equations (in rheological view) for an isotropic and incompressible Casson liquid motion is

$$T_{ij} = \begin{cases} 2\big(\mu_P + p_y/\sqrt{2\Pi}\,\big)e_{ij}; & \Pi > \Pi_c \\ 2\big(\mu_P + p_y/\sqrt{2\Pi_c}\,\big)e_{ij}; & \Pi < \Pi_c. \end{cases} \tag{1}$$

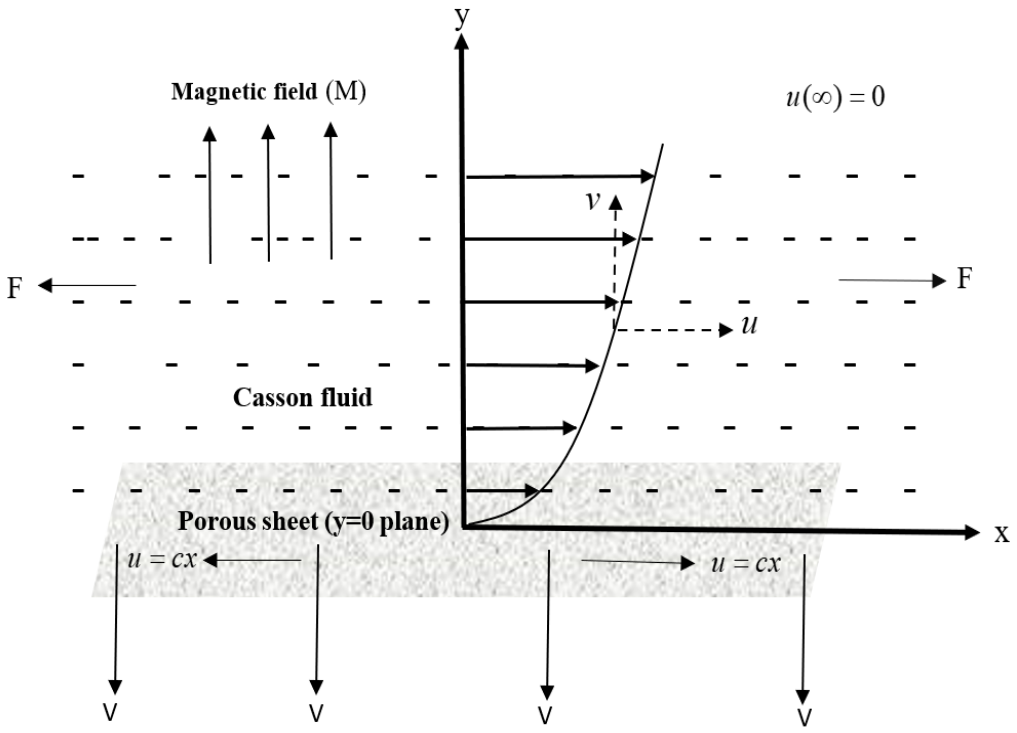

Figure 1: Sketch of the problem

In the presence of uniform magnetic field, fundamental boundary layer equations for steady, isotropic and incompressible Casson fluid flow, introduced by a great German fluid dynamicist Ludwig Prandtl, are

$$\left(\frac{\mu_P}{k}\right)u + \rho\left[u\left(\frac{\partial u}{\partial x}\right) + v\left(\frac{\partial u}{\partial y}\right)\right] = \left(\mu_P + \frac{p_y}{\sqrt{2\Pi_c}}\right)\left(\frac{\partial^2 u}{\partial y^2}\right) - \sigma M^2 u, \tag{2}$$

$$\left(\frac{\partial u}{\partial x}\right) + \left(\frac{\partial v}{\partial y}\right) = 0, \tag{3}$$

where the mathematical symbols σ, ρ, M and k stand for the electrical conductivity, fluid density, magnetic field and permeability of porous medium, respectively.

2.1 Solution of problem

As per characteristics of fluid, if a shear stress T_{ij} greater than yield stress p_y is applied, then fluid motion occurs while fluid will behave like a non-deformable object (*i.e.* solid) if $T_{ij} < p_y$. Introducing a scalar valued function $\psi(x, y)$ connecting with velocity components u and v so that equation of continuity (3) is satisfied. For this, we may take

$$u = \frac{\partial \psi}{\partial y} \qquad \text{and} \qquad v = -\frac{\partial \psi}{\partial x}. \tag{4}$$

Transforming the variable y in the new variable η as follows

$$\eta = y\sqrt{\frac{c\rho}{\mu_P}} \qquad \text{and} \qquad \psi(x,\eta) = xf(\eta)\sqrt{\frac{c\mu_P}{\rho}}. \tag{5}$$

Therefore, we have the velocity components in terms of new variable η will be

$$u = cxf'(\eta), \qquad v = -f(\eta)\sqrt{\frac{c\mu_P}{\rho}}. \tag{6}$$

Substituting the values of y, ψ, u and v in the equation (2), we have

$$f'^2(\eta) - f(\eta)f''(\eta) = \left[1 + \frac{1}{\beta}\right]f'''(\eta) - Hf'(\eta), \tag{7}$$

where, $\quad H = \dfrac{1}{c}\left(\dfrac{\nu}{k} + \dfrac{\sigma M^2}{\rho}\right), \quad \nu = \dfrac{\mu_P}{\rho}, \quad \beta = \dfrac{\mu_P\sqrt{2\Pi_c}}{p_y}.$

The above mentioned symbol β is Casson fluid parameter and ν represents kinematic viscosity coefficient.

2.2 Boundary conditions

Assuming that V is the suction velocity at the wall, then as per geometry of the mathematical problem, we have the appropriate boundary conditions:

$$u = cx \ \text{ at } y = 0; \qquad v = -V \ \text{ at } y = 0 \qquad \text{and} \qquad u \to 0 \text{ as } y \to \infty.$$

Restating the above mentioned boundary conditions in the terms of variable η as:

$$f'(\eta) = 1 \ \text{ at } \eta = 0; \qquad f(\eta) = R \ \text{ at } \eta = 0 \qquad \text{and} \qquad f'(\eta) \to 0 \text{ as } \eta \to \infty, \tag{8}$$

where R is the suction parameter which is given by $R = V/\sqrt{\nu c}$.

2.3 Analysis on exactness of solution

A hypothetical solution for the boundary value problem *i.e.* non-linear differential equation (7) with boundary conditions (8) can be taken as follows:

$$f(\eta) = A + B\ exp(-\alpha\eta), \tag{9}$$

where A, B and α are unknowns that are to be evaluated with $\alpha > 0$.

Substituting the expression of $f(\eta)$ from equation (9) into the equation (7) and then equating $\eta \to 0$ both sides, we obtain

$$A = \alpha\left(1 + \frac{1}{\beta}\right) - \frac{H}{\alpha}. \tag{10}$$

Due to exponential term in the expression of $f(\eta)$ and on the basis of boundary conditions (8), we have

$$B = -\frac{1}{\alpha} \quad \text{and} \quad A + B = R. \tag{11}$$

The values of α can be determined in two equivalent ways:

$$\alpha = \frac{R\beta + \sqrt{R^2\beta^2 + 4\beta(H+1)(\beta+1)}}{2(\beta+1)} \quad \text{and} \quad \alpha = \frac{A\beta + \sqrt{A^2\beta^2 + 4H\beta(\beta+1)}}{2(\beta+1)}. \tag{12}$$

For further analysis, we wish to use former value of α, and therefore, we have obtained the unique values of A and B, and these values are

$$A = \frac{R\beta(2H+1) + \sqrt{R^2\beta^2 + 4\beta(H+1)(\beta+1)}}{2\beta(H+1)}$$

and

$$B = \frac{R\beta - \sqrt{R^2\beta^2 + 4\beta(H+1)(\beta+1)}}{2\beta(H+1)}.$$

2.4 Expressions of velocity components u and v

Substituting the value of $f(\eta)$ in the equations (5) and (6), we obtain the stream function:

$$\psi(x,\eta) = \frac{x\sqrt{\nu c}}{2\beta(H+1)}\Bigg[R\beta(2H+1) + \sqrt{R^2\beta^2 + 4\beta(H+1)(\beta+1)} + \left(R\beta - \sqrt{R^2\beta^2 + 4\beta(H+1)(\beta+1)}\right)e^{-\alpha\eta}\Bigg]. \tag{13}$$

Velocity components are

$$u(x,\eta) = cx\ exp\left[-\frac{\eta\left(R\beta + \sqrt{R^2\beta^2 + 4\beta(H+1)(\beta+1)}\right)}{2(\beta+1)}\right] \tag{14}$$

and

$$v(x,\eta) = -\frac{\sqrt{\nu c}}{2\beta(H+1)}\Bigg[R\beta(2H+1) + \sqrt{R^2\beta^2 + 4\beta(H+1)(\beta+1)} + \left(R\beta - \sqrt{R^2\beta^2 + 4\beta(H+1)(\beta+1)}\right)e^{-\alpha\eta}\Bigg]. \tag{15}$$

2.5 Determination of skin friction coefficient

The skin friction coefficient at plane (*i.e.* $y = 0$) is given by $f''(0)$. So, we have

$$f''(0) = -\frac{R\beta + \sqrt{R^2\beta^2 + 4\beta(H+1)(\beta+1)}}{2(\beta+1)}. \tag{16}$$

3 Special cases of flow analysis

Case-I:

When permeability parameter $k \to \infty$ and the effect of magnetic field is vanishing, *i.e.* $\sigma \to 0$, then

$$f(\eta) \to \frac{-2(\beta+1)\exp\left(-\frac{\eta(\sqrt{\beta}\sqrt{\beta(R^2+4)+4}+\beta R)}{2(\beta+1)}\right) + \beta(R^2+2) + \sqrt{\beta}R\sqrt{\beta(R^2+4)+4} + 2}{\sqrt{\beta}\sqrt{\beta(R^2+4)+4} + \beta R},$$

$$f'(\eta) \to \exp\left(-\frac{\eta\left(\sqrt{\beta}\sqrt{\beta\left(R^2+4\right)+4} + \beta R\right)}{2(\beta+1)}\right),$$

$$f''(0) \to -\frac{\sqrt{\beta}\sqrt{\beta\left(R^2+4\right)+4} + \beta R}{2(\beta+1)}.$$

This result matches with the result published by Mukhopadhyay *et al.* (2013).

Case-II:

When both Casson parameter β and permeability parameter k are tending to infinity, *i.e.* $\beta \to \infty$ and $k \to \infty$, then

$$f(\eta) \to \frac{-2\ exp\Big[-\frac{1}{2}\eta\left(\sqrt{\frac{4B^2\sigma}{c\rho} + R^2 + 4} + R\right)\Big] + R\left(\sqrt{\frac{4B^2\sigma}{c\rho} + R^2 + 4} + R\right) + 2}{\sqrt{\frac{4B^2\sigma}{c\rho} + R^2 + 4} + R},$$

$$f'(\eta) \to exp\left[-\frac{1}{2}\eta\left(\sqrt{\frac{4B^2\sigma}{c\rho} + R^2 + 4} + R\right)\right],$$

$$f''(0) \to \frac{1}{2}\left(-\sqrt{\frac{4B^2\sigma}{c\rho} + R^2 + 4} - R\right).$$

This result matches with the result reported by Chakraborti and Gupta (1979), Vajravelu and Rollins (1992) and Pop and Na (1998).

Case-III:

When electrical conductivity σ is approaching to zero and Casson parameter β is tending to infinity, *i.e.* $\sigma \to 0$ and $\beta \to \infty$, then

$$f(\eta) \to \frac{-2\ exp\Big[-\frac{1}{2}\eta\left(\sqrt{\frac{4\nu}{ck}+R^2+4}+R\right)\Big]+R\left(\sqrt{\frac{4\nu}{ck}+R^2+4}+R\right)+2}{\sqrt{\frac{4\nu}{ck}+R^2+4}+R},$$

$$f'(\eta) \to exp\Big[-\frac{1}{2}\eta\left(\sqrt{4H+R^2+4}+R\right)\Big],$$

and
$$f''(0) \to \frac{1}{2}\left(-\sqrt{4H+R^2+4}-R\right).$$

This result matches with the result reported earlier by Chamkha *et al.* (2010) and Mukhopadhyay (2009).

Case-IV:

When Casson parameter β is tending to infinity, porous medium is removed ($k \to \infty$) and electrical conductivity σ due to external magnetic field is absent, *i. e.* $\beta \to \infty$, $k \to \infty$ and $\sigma \to 0$, then

$$f(\eta) \to \frac{-2\ exp\big[-\frac{1}{2}\eta\left(R+\sqrt{R^2+4}\right)\big]+R\left(R+\sqrt{R^2+4}\right)+2}{R+\sqrt{R^2+4}},$$

$$f'(\eta) \to exp\left[-\frac{1}{2}\eta\left(R+\sqrt{R^2+4}\right)\right],$$

and
$$f''(0) \to -\frac{1}{2}\left(R+\sqrt{R^2+4}\right).$$

This result is valid and the same result was reported earlier by Mukhopadhyay (2011) and Kumaran *et al.* (1996).

Case-V:

When permeability k becomes infinite, *i. e.* $k \to \infty$, then

$$f(\eta) \to \frac{-2(\beta+1)\ exp\left(-\frac{\eta(\beta R+\Gamma)}{2(\beta+1)}\right)+R\Gamma+\beta\left(R^2+2\right)+2}{\beta R+\Gamma}, \tag{17}$$

$$f'(\eta) \to \exp\left(-\frac{\eta\left(\Gamma+\beta R\right)}{2(\beta+1)}\right),$$

$$f''(0) \to -\frac{\Gamma+\beta R}{2(\beta+1)},$$

where
$$\Gamma = \left(\sqrt{\beta}\sqrt{\frac{4(\beta+1)M^2\sigma}{c\rho}+\beta\left(R^2+4\right)+4}\ \right).$$

This result matches with the result reported by Bhattacharyya *et al.* (2013).

Case-VI:

When Casson parameter $\beta \to \infty$, then behavior of Casson fluid coincides with the Newtonian fluid characteristics. Therefore,

$$f(\eta) \to \frac{-2e^{-\frac{1}{2}\eta\left(\sqrt{4H+R^2+4}+R\right)} + R\left(\sqrt{4H+R^2+4}+R\right)+2}{\sqrt{4H+R^2+4}+R},$$

$$f'(\eta) \to exp\left[-\frac{1}{2}\eta\left(\sqrt{4H+R^2+4}+R\right)\right],$$

$$f''(0) \to \frac{1}{2}\left(-\sqrt{4H+R^2+4}-R\right).$$

Case-VII:

When magnetic field is removed, *i.e.* $\sigma \to 0$, then

$$f(\eta) \to \frac{-2(\beta+1)\exp\left(-\frac{\eta(\chi+\beta R)}{2(\beta+1)}\right) + R\chi + \beta\left(R^2+2\right)+2}{\chi+\beta R},$$

$$f'(\eta) \to \exp\left(-\frac{\eta\left(\chi+\beta R\right)}{2(\beta+1)}\right),$$

$$f''(0) \to -\frac{\chi+\beta R}{2(\beta+1)},$$

where $$\chi = \sqrt{\beta}\sqrt{\frac{4(\beta+1)\nu}{ck} + \beta\left(R^2+4\right)+4}.$$

4 Results and Discussion

In this section, we will discuss the graphical behavior of horizontal velocity $f'(\eta)$, the transverse velocity $f(\eta)$ and skin friction coefficient $f''(0)$ on the different flow parameters, like Casson parameter β, parameter c, permeability parameter k, electrical conductivity σ, suction velocity V. Some values of flow parameters are chosen fixed such as kinematic viscosity ($\nu = 10$), external magnetic field $M = 3$ and fluid density $\rho = 0.2$. In graphs of velocities, variation in parameter η ($0 \leq \eta \leq 3$) and in the plot of skin friction coefficient, magnetic field parameter M ($0 \leq M \leq 3$) are considered.

4.1 Effects of Casson Parameter (β)

Fluid velocity profiles $f'(\eta)$ and $f(\eta)$ are plotted against the parameter η and the skin friction coefficient $f''(0)$ are plotted against magnetic parameter M whose graphical characteristics are explained for different values of Casson fluid parameter β when electrical conductivity is $\sigma = 0.2$.

Horizontal velocity profile $f'(\eta)$

The profiles of horizontal velocity are plotted for the values of $c = 2$, permeability parameter $k = 5$, suction velocity $V = 0.01$ and magnetic field $M = 3$. As the Casson parameter increases, then the velocities decreases and follows the Newtonian fluid behaviors. On the other hand, if we take the variation of η, then the fluid motion is decaying in an asymptotic behavior. The axis of η is acting as an asymptote of these velocity profiles (Figure 2).

Transverse velocity profile $f(\eta)$

Transverse velocity graphs (Figure 3) are plotted for the values of permeability parameter $k = 0.75$, suction velocity $V = 0.01$, non-negative parameter $c = 3$ and magnetic field $M = 3$. As the Casson parameter increases, then the velocity decreases and follows the Newtonian fluid behaviors. As we are observing the graph of $f(\eta)$ with the variation of η, then we obtain that the velocity is increasing for all values of β whenever $\eta \leq 2$. Also, as we are moving beyond $\eta \geq 2$, the transverse velocity is varying uniformly.

Skin friction coefficient $f''(0)$

Here, we plot graphs of skin friction coefficient $f''(0)$ with respect to magnetic parameter $M(0 \leq M \leq 3)$ for the values of suction velocity $V = 0.1$, permeability parameter $k = 0.75$ and non-negative parameter $c = 3$. The skin friction coefficient $f''(0)$ decreases as the Casson parameter β increases and further decreasing slowly as the magnetic parameter M is increasing (Figure 4).

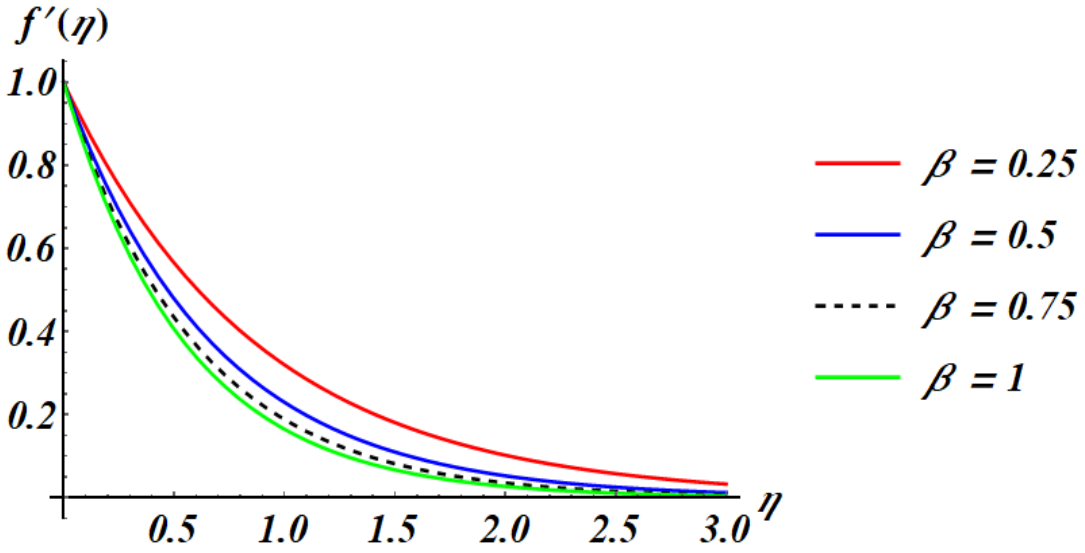

Figure 2: Horizontal velocity profile $f'(\eta)$ when Casson parameter $\beta = 0.25, 0.5, 0.75, 1$.

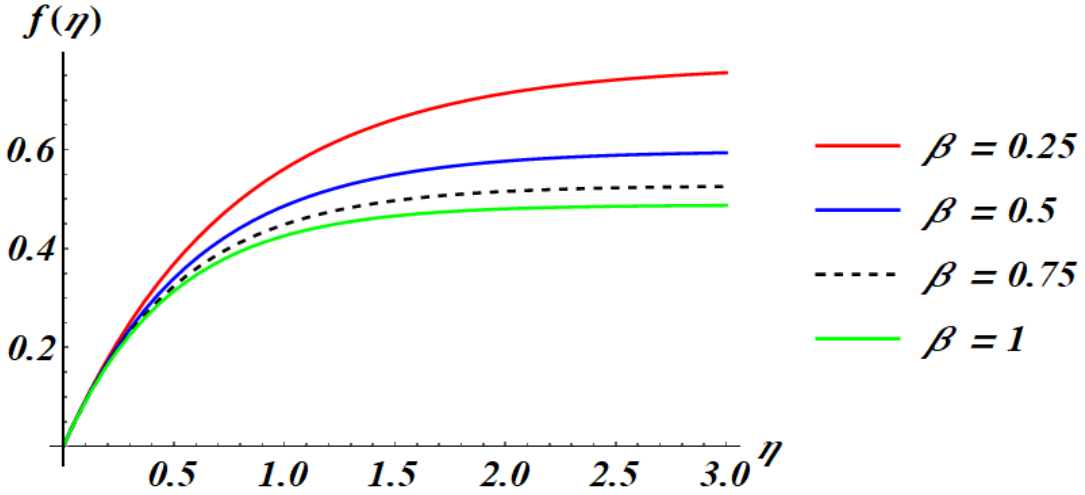

Figure 3: Transverse velocity profile $f(\eta)$ when Casson parameter $\beta = 0.25, 0.5, 0.75, 1$.

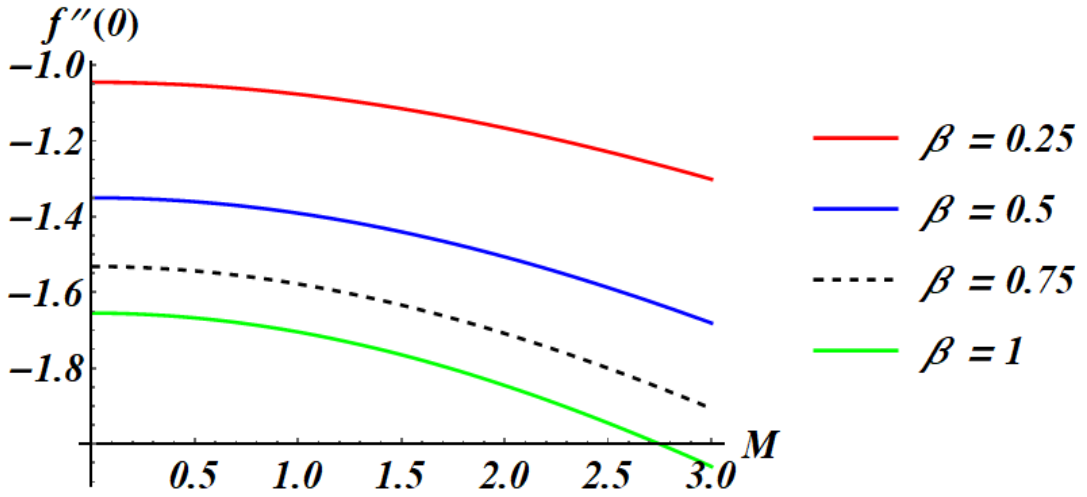

Figure 4: Skin friction coefficient $f''(0)$ when Casson parameter $\beta = 0.25, 0.5, 0.75, 1$.

4.2 Effects of non-Negative Parameter (c)

Profiles of horizontal velocity $f'(\eta)$ and transversal velocity $f(\eta)$ are plotted against η. Further, the sketch of skin friction coefficient is drawn against magnetic parameter M. The graphical nature for different values of c are investigated by taking $\sigma = 0.2$.

Horizontal velocity profile $f'(\eta)$

The component of fluid velocity (Figure 5) along x-axis is plotted with the Casson parameter $\beta = 0.2$, parameter $k = 2$, suction velocity $V = 0.01$ and magnetic field $M = 3$. As the parameter c increases, then the profile of such velocity increases. Along with the variation of parameter η, the graph is decreasing whenever $\eta \leq 2$ and after then, it is varying slowly. Also, the axis of η is become an asymptote of $f'(\eta)$.

Transverse velocity profile $f(\eta)$

The fluid velocity component $f'(\eta)$ is plotted when the Casson parameter is $\beta = 0.5$, parameter $k = 0.75$, suction velocity is $V = 0.01$ and magnetic field is $M = 3$. Profile of $f(\eta)$ increases upto a critical value and moving uniformly as the non-negative parameter c increasing. The velocity components (Figure 6) are further varying constantly whenever $\eta \geq 2$.

Skin friction coefficient $f''(0)$

The graphical nature of skin friction coefficient $f''(0)$ is shown in the figure 7 versus magnetic parameter $M(0 \leq M \leq 3)$. The values of suction velocity $V = 0.1$, permeability parameter is $k = 0.75$ and non-negative parameter $c = 3$ are taken fixed. The profile of friction coefficient $f''(0)$ increases as the parameter c increases. When the value of c is becoming large, then graphs are contracting and decreasing slowly as the magnetic field parameter M increases.

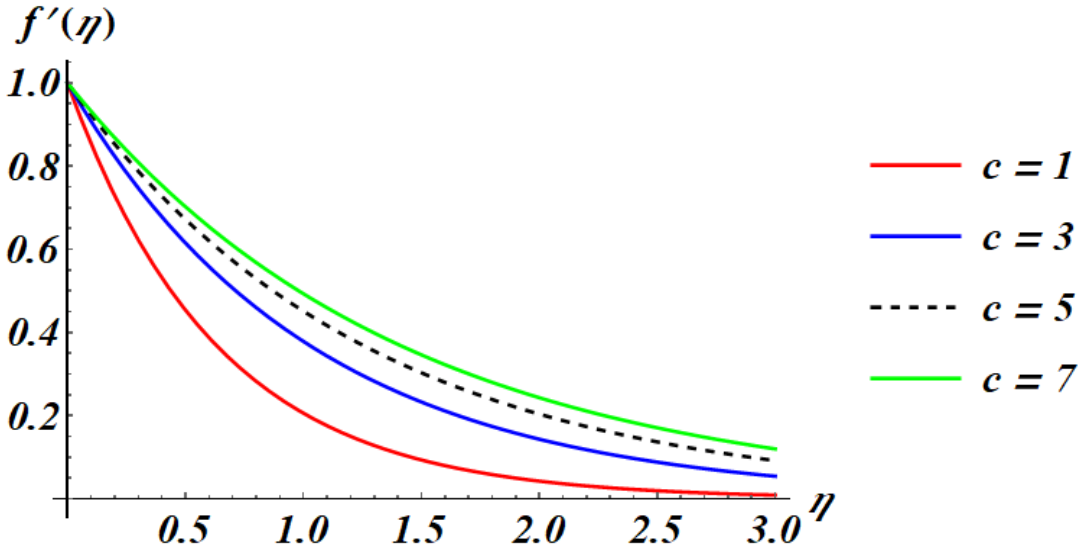

Figure 5: Horizontal velocity profile when $c = 1, 3, 5, 7$.

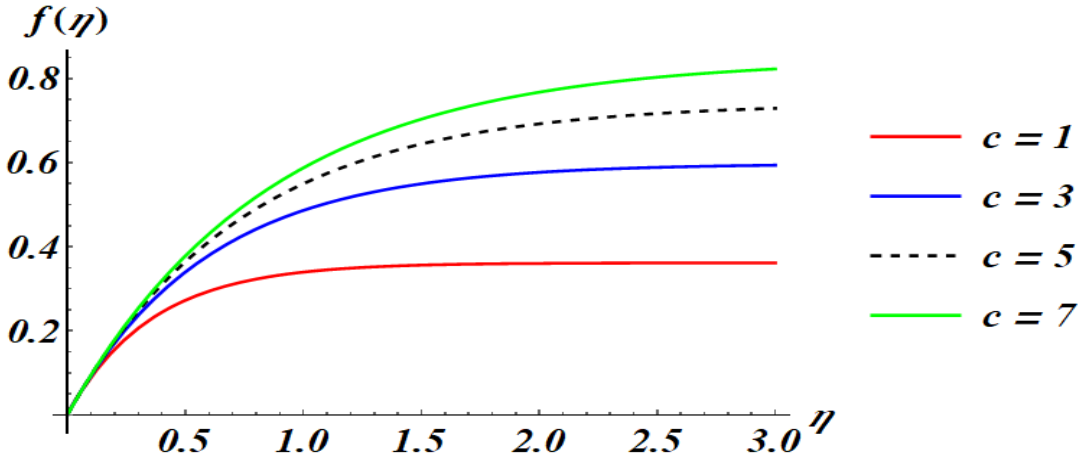

Figure 6: Transverse velocity profile when $c = 1, 3, 5, 7$.

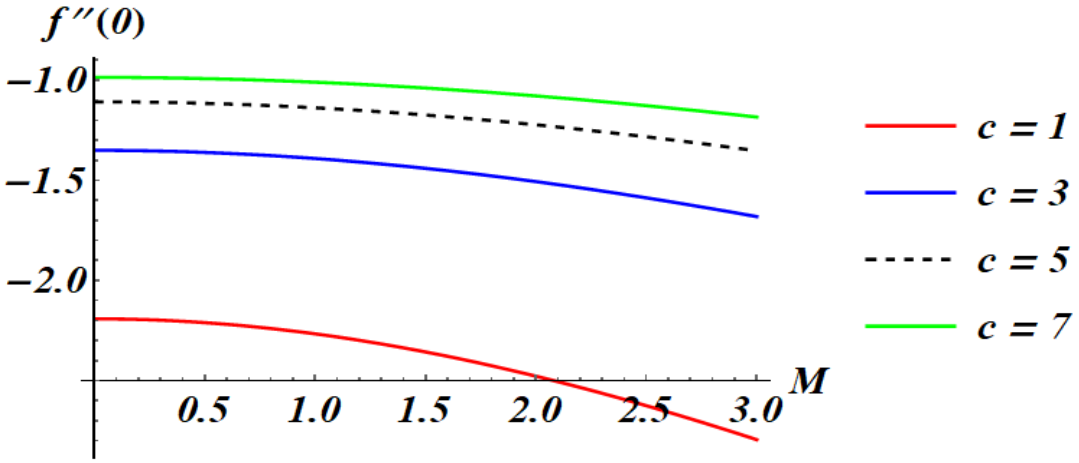

Figure 7: Skin friction coefficient $f''(0)$ when $c = 1, 3, 5, 7$.

4.3 Effects of Permeability Parameter (k)

Sketches of skin friction coefficient $f''(0)$, transversal velocity $f(\eta)$ and profile of horizontal velocity $f'(\eta)$ are plotted and their graphical behaviors are also discussed for different values of k by taking $\sigma = 0.2$.

Horizontal velocity profile $f'(\eta)$

The graphs of velocity (Figure 8) along x-axis are plotted when $\beta = 0.2$, $c = 2$, $V = 0.01$ and magnetic field $M = 3$. As the permeability k increases, the horizontal velocity increases. Along with the variation of parameter η, the graph is decreasing slowly upto a critical limit and then varies in such a way that the η-axis is become an asymptote.

Transverse velocity profile $f(\eta)$

The graph of transverse velocity (Figure 9) is sketched using $\beta = 0.2$, $c = 2$, $M = 3$ and $V = 0.01$. Velocity profile is increasing as the permeability parameter k increases. With the large variation in η, the graph is varying constantly.

Skin friction coefficient $f''(0)$

The graphical view of $f''(0)$ is reported versus parameter $M(0 \leq M \leq 3)$ using the values of velocity $V = 0.1$, parameter is $c = 3$ and Casson parameter $\beta = 0.25$ are taken. Figure 10 shows that the graph of skin friction coefficient $f''(0)$ increases as the permeability parameter k increases. Whenever the value of magnetic parameter M is varying, then skin friction coefficient are decaying very slowly.

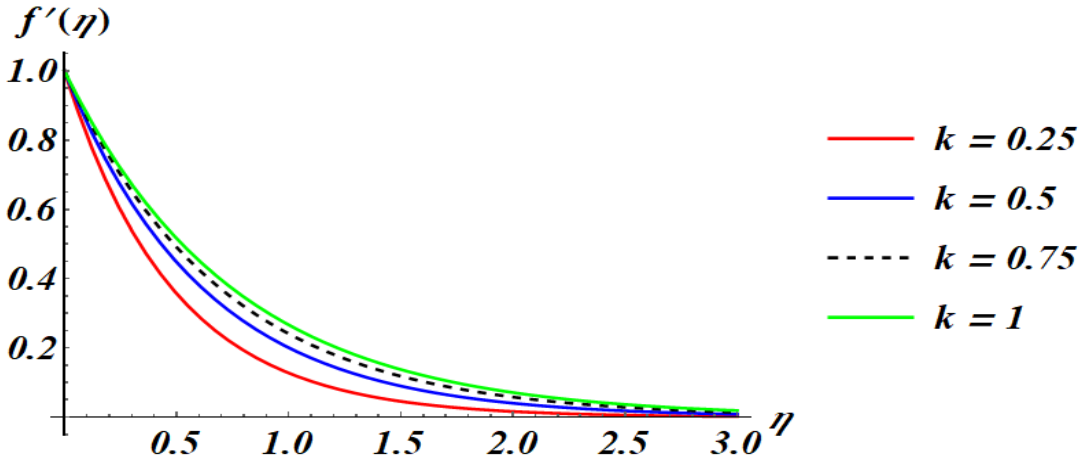

Figure 8: Horizontal velocity profile when permeability $k = 0.25, 0.5, 0.75, 1$.

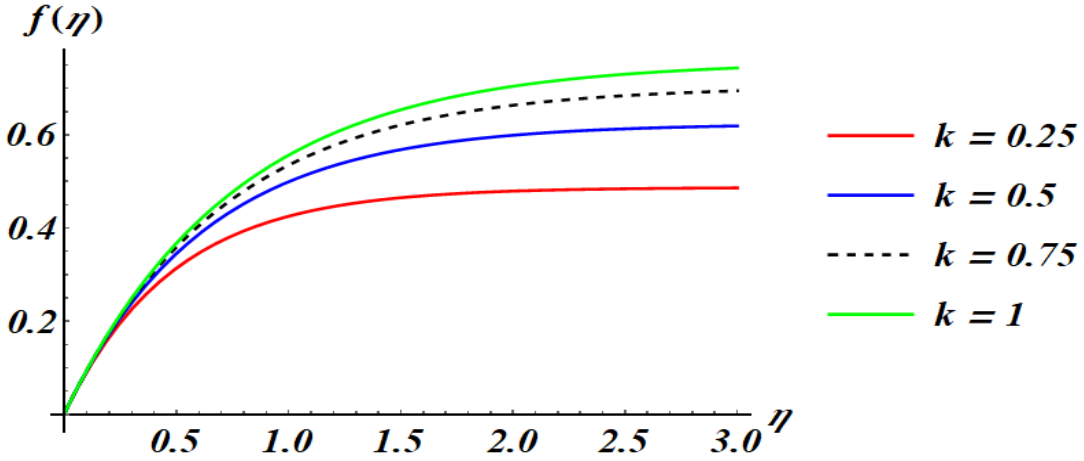

Figure 9: Transverse velocity profile $f(\eta)$ when permeability $k = 0.25, 0.5, 0.75, 1$.

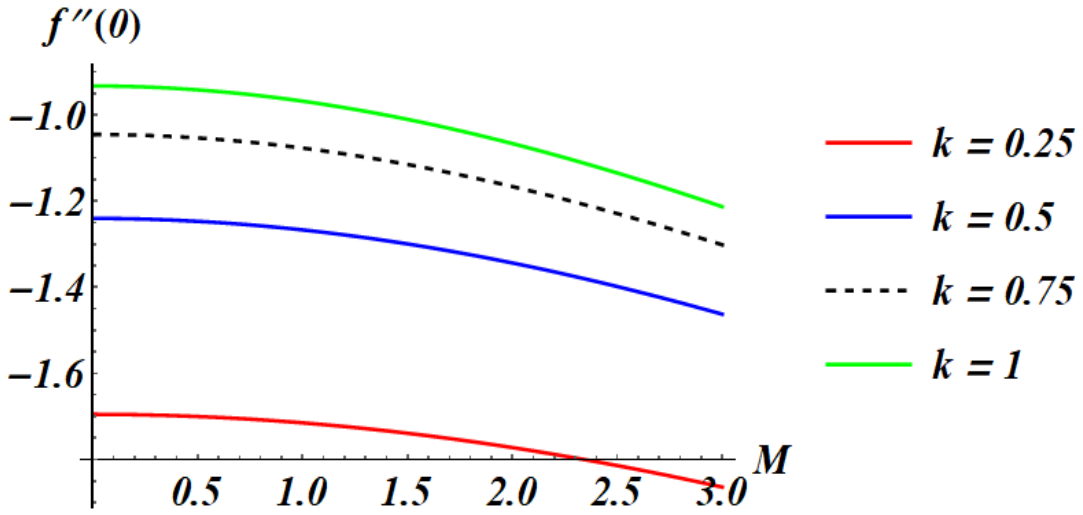

Figure 10: Skin friction coefficient $f''(0)$ when permeability $k = 0.25, 0.5, 0.75, 1$.

4.4 Effects of Electrical Conductivity (σ)

Horizontal velocity profile $f'(\eta)$

The profile of horizontal velocity versus length parameter η varying from 0 to 3 is drawn with $\beta = 0.2$, $c = 2$, $V = 0.01, k = 0.75$ and magnetic field parameter $M = 3$. Figure 11 represents that velocity profile is decreasing whenever we are moving far away in the upwards direction to the stretching sheet. With the increasing value of electrical conductivity σ, horizontal velocity is decreasing.

Transverse velocity profile $f(\eta)$

The transversal velocity's graph (Figure 12) versus η is plotted using the numerical values of flow parameters $\beta = 0.2$, $c = 2$, $V = 0.01, k = 0.2$ and $M = 3$. Velocity graph can be observed in two ways. The velocity profile is decreasing whenever conductivity parameter σ is increasing. On the other hand, graph of this velocity increasing rapidly for small values of η and for the large value of η, profile is varying uniformly.

Skin friction coefficient $f''(0)$

The plot of friction coefficient against M is drawn using the values of $\beta = 0.25$, $c = 3$, $V = 0.1, k = 0.75$. Graph of friction coefficient is decreasing as the electrical conductivity σ is increasing. The curves of $f''(0)$ is diverging as the values of magnetic parameter M is being large (Figure 13).

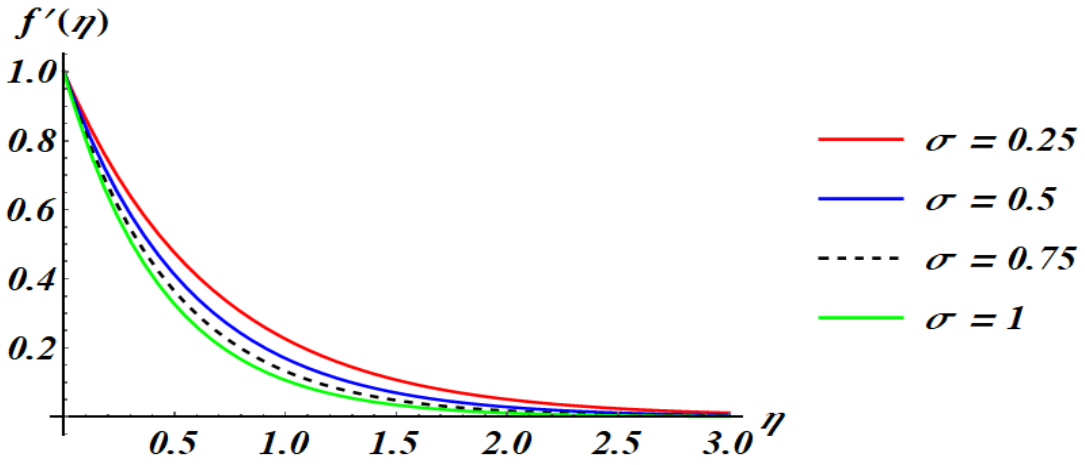

Figure 11: Horizontal velocity $f'(\eta)$ when electrical conductivity $\sigma = 0.25, 0.5, 0.75, 1$.

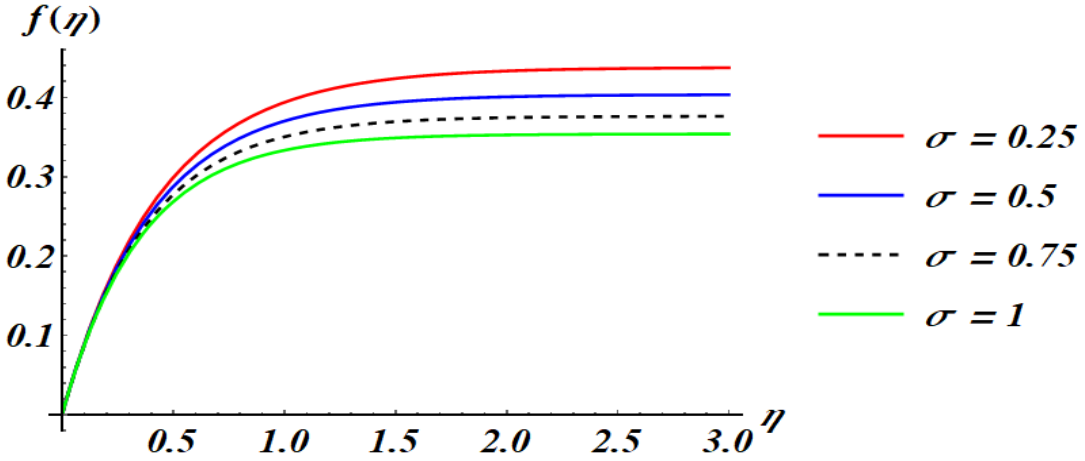

Figure 12: Transverse velocity $f(\eta)$ when electrical conductivity $\sigma = 0.25, 0.5, 0.75, 1$.

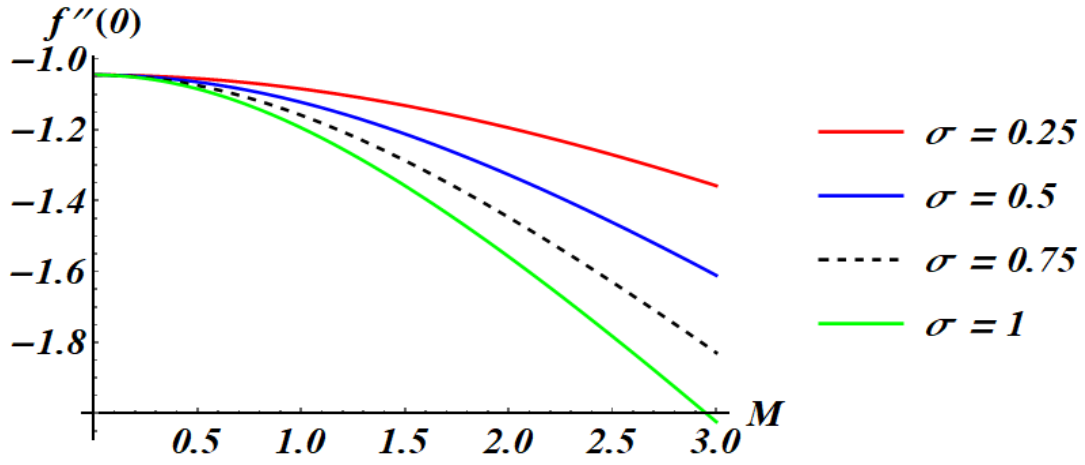

Figure 13: Skin friction coefficient $f''(0)$ when electrical conductivity $\sigma = 0.25, 0.5, 0.75, 1$.

4.5 Effects of Suction Velocity (V)

Geometrical view of horizontal velocity $f'(\eta)$, transversal velocity $f(\eta)$ and skin friction coefficient $f''(0)$ are drawn and their behaviors are explained for different values of suction velocity V by taking $\sigma = 0.2$.

Horizontal velocity profile $f'(\eta)$

Graphs of horizontal velocity are sketched against the length parameter η varies from 0 to 3 when $\beta = 0.2$, $c = 2, k = 5$ and $M = 3$. Figure 14 exhibits that the velocity profiles are decreasing sharply whenever $\eta \leq 2$ and for the large values of η, it is decaying slowly and η-axis is become an asymptote of velocity graphs. For the increasing value of suction velocity V, profiles of the horizontal velocity are decreasing.

Transverse velocity profile $f(\eta)$

Profiles of velocity $f(\eta)$ are plotted against η which is lying between 0 to 3 for $\beta = 0.2$, $c = 2, k = 0.75$ and $M = 3$. Transverse velocity is increasing very slowly for small value of η and for the large values of η, it varies uniformly. As the value of suction velocity V increases, profile of the transverse velocity increases (Figure 15).

Skin friction coefficient $f''(0)$

Graphs (Figure 16) of skin friction coefficient $f''(0)$ are plotted against magnetic field parameter M which is varying from 0 to 3 for $\beta = 0.5$, $c = 3, k = 0.75$. When the suction velocity increases, then skin friction coefficient $f''(0)$ decreases. Whenever the value of magnetic parameter M is tending to unity, then graph of $f''(0)$ is varying uniformly and for the large values of M, it is decreasing rapidly with the variation of η.

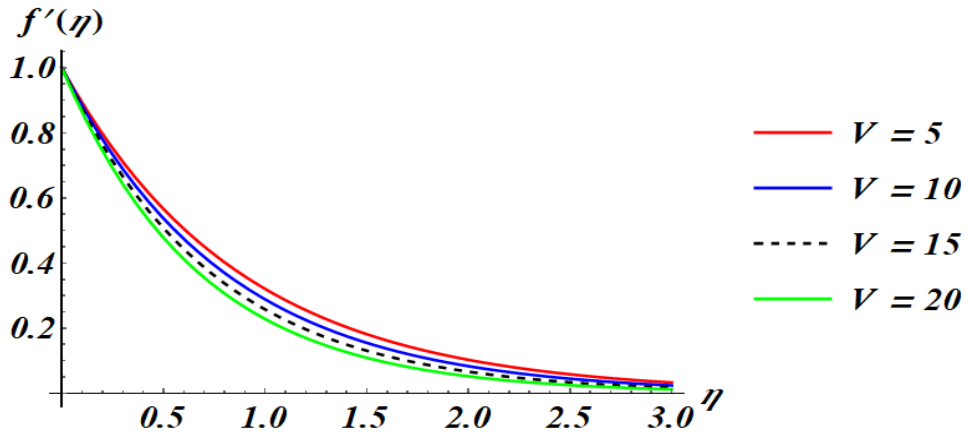

Figure 14: Horizontal velocity profile $f'(\eta)$ when suction velocity $V = 5, 10, 15, 20$.

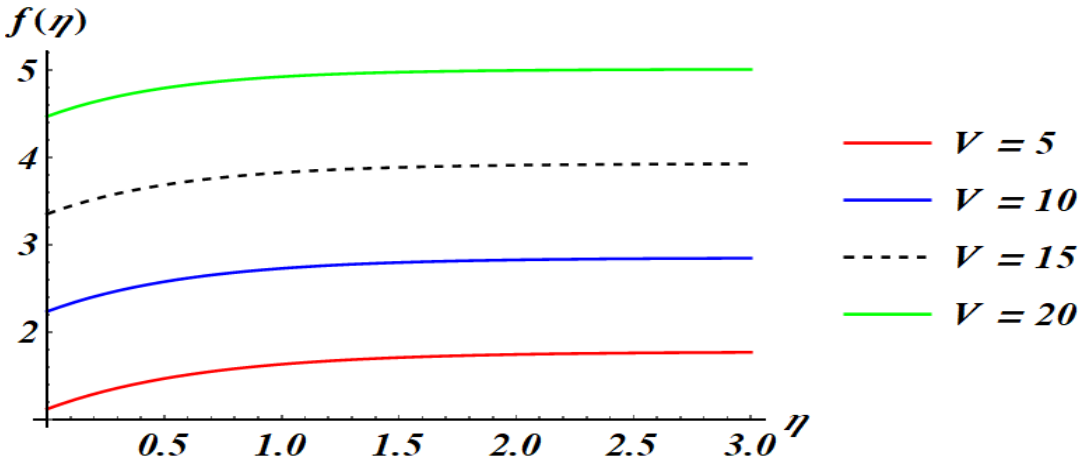

Figure 15: Transverse velocity profile $f(\eta)$ when suction velocity $V = 5, 10, 15, 20$.

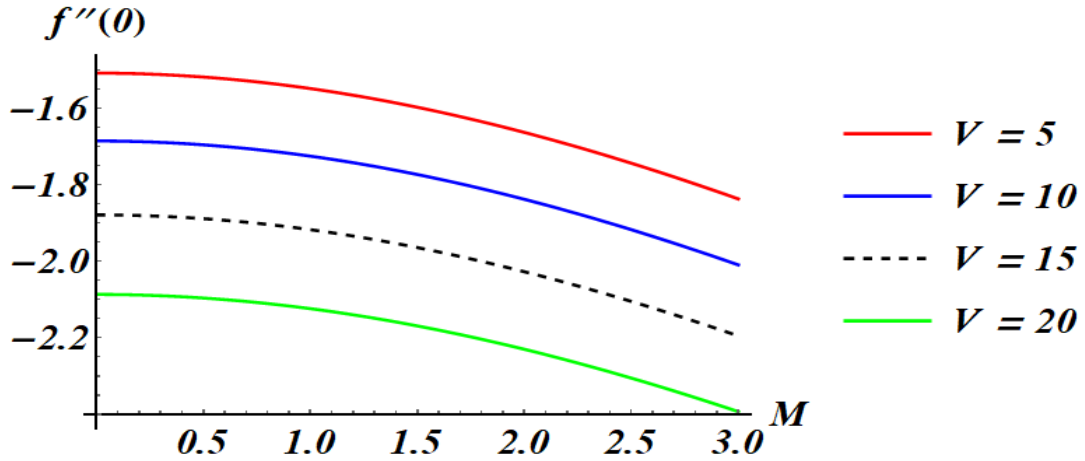

Figure 16: Skin friction coefficient $f''(0)$ when suction velocity $V = 5, 10, 15, 20$.

5 Conclusion

In the present research work, magnetohydrodynamic effect of Casson fluid flowing over a porous stretching sheet ($y = 0$) is investigated. The fluid flow problem leads into a non-linear ordinary differential equation which is solved by MATHEMATICA software. Fluid velocity components (horizontal and transversal), skin friction coefficient are determined using relevant boundary conditions. Special cases of present study for horizontal velocity, transverse velocity and skin friction coefficient are deduced. Profiles of the velocity components and skin friction coefficient are plotted for different values of flow parameters, such as, Casson parameter, suction velocity, electrical conductivity, permeability

parameter, etc.

For particularly large values of Casson parameter β, Casson fluid behaves like a Newtonian fluid. The effect of Casson parameter with increasing value suppresses the flow field. On the other hand, the role of increasing/decreasing value of permeability parameter is to suppress the velocity field of an incompressible viscous fluid. This work can find mechanical applications in polymer technology and metallurgy (hydromagnetic techniques). The work can be utilized to control the cooling/heating rate in electrically conducting flows. From the above investigation, the main conclusions are summarized as follows:

- The velocity component (horizontal) is decreasing function of Casson parameter, suction velocity and magnetic parameter (*i.e.* electrical conductivity).
- The transversal velocity component is decreasing function of Casson parameter and electrical conductivity, but not of suction velocity.
- The value of skin friction coefficient $f''(0)$ grows either as the permeability parameter k or non-negative parameter c increases, and decreases either as the Casson parameter β or conductivity σ or suction velocity V increases.

Declarations

Ethical Approval

Not Applicable

Competing interests

Authors declare that they have no competing interests.

Authors' contributions

Dr. Deepak K. Maurya developed the problem's mathematical model and performed an analytical assessment as the first author. Prof. Satya Deo validates the obtained data and graphs. Dr. Pankaj Kumar Maurya checks over the writing and vocabulary yet another time.

Funding

No funding.

Availability of data and materials

On reasonable request, the corresponding author will provide the datasets developed during the current work.

References

[1] Abdus, S.S. and Sharif, U., *MHD Boundary Layer Casson Fluid Over a Nonlinear Stretching Sheet*, Lambert Academic Publishing, 2015.

[2] Lukaszewicz, G., *Micropolar Fluids: Theory and Applications*, New York: Springer, 1999.

[3] Stokes, V.K., *Theories of Fluids with Microstructure*, New York: Springer, 1984.

[4] Rott, N., Unsteady Viscous Flow in the Vicinity of a Stagnation Point, *Quart. Appl. Math.*, vol. **13**, no. 4, pp. 444-451, 1956.

[5] Bluman, G.W. and Cole, J.D., *Similarity Methods for Differential Equations*, Springer, 1974.

[6] Chakraborti, A. and Gupta, A.S., Hydromagnetic Flow and Heat Transfer Over a Stretching Sheet, *Quart. Appl. Math.*, vol. **37**, no. 1, pp. 73-78, 1979.

[7] Vajravelu, K. and Rollins, D., Heat Transfer in an Electrically Conducting Fluid Over a Stretching Surface, *Int. J. Non-Linear Mech.*, vol. **27**, no. 2, pp. 265-277, 1992.

[8] Chamkha, A.J., Aly, A.M. and Mansour, M.A., Similarity Solution for Unsteady Heat and Mass Transfer from a Stretching Surface Embedded in a Porous Medium with Suction/Injection and Chemical Reaction Effects, *Chem. Eng. Comm.*, vol. **197**, no. 6, pp. 846–858, 2010.

[9] Arthur, E.M., Seini, I.Y. and Bortteir, L.B., Analysis of Casson Fluid Flow Over a Vertical Porous Surface with Chemical Reaction in the Presence of Magnetic Field, *J. Appl. Math. Phy.*, vol. **3**, pp. 713-723, 2015.

[10] Rasool, G., Chamkha, A.J., Muhammad, T., Shafiq, A. and Khan, I., Darcy-Forchheimer Relation in Casson Type MHD Nanofluid Flow Over Non-linear Stretching Surface, *Propuls. Power Res.*, vol. **9**, no. 2, pp. 159-168, 2020.

[11] Krishna, M.V., Reddy, M.G. and Chamkha, A.J., Heat and Mass Transfer on MHD Free Convective Flow Over an Infinite Nonconducting Vertical Flat Porous Plate, vol. **46**, no. 1, pp. 1-25, 2019.

[12] Krishna, M.V. and Chamkha, A.J., Hall and Ion Slip Effects on MHD Rotating Boundary Layer Flow of Nanofluid Past an Infinite Vertical Plate Embedded in a Porous Medium, *Results Phys.*, vol. **15**, Article no. 102652, 2019.

[13] Medikare, M., Joga, S. and Chidem, K.K., MHD Stagnation Point Flow of a Casson Fluid Over a Nonlinearly Stretching Sheet with Viscous Dissipation, *Amer. J. Comput. Math.*, vol. **6**, pp. 37-48, 2016.

[14] Nanjundaswamy, V.K.P., Mahabaleshwar, U.S., Mallikarjun, P., Nezhad, M.M. and Lorenzini, G., Casson Liquid Flow due to Porous Stretching Sheet with Suction/Injection, *Defect. Diffusion Forum*, vol. **388**, pp. 420-432, 2018.

[15] Akbar, N., Hussain, S.M. and Khan, R.U., Numerical Solution of Casson Fluid Flow under Viscous Dissipation and Radiation Phenomenon, *J. Appl. Math. Phy.*, vol. **10**, pp. 475-490, 2022.

[16] Mukhopadhyay, S., Effect of Thermal Radiation on Unsteady Mixed Convection Flow and Heat Transfer Over a Porous Stretching Surface in Porous Medium, *Int. J. Heat Mass Transf.*, vol. **52**, nos. 13-14, pp. 3261–3265, 2009.

[17] Mukhopadhyay, S., Effects of Slip on Unsteady Mixed Convective Flow and Heat Transfer Past a Porous Stretching Surface, *Nucl. Eng. Des.*, vol. **241**, no. 8, pp. 2660– 2665, 2011.

[18] Mukhopadhyay, S., De, P.R. and Bhattacharya, K., Casson Fluid Flow Over an Unsteady Stretching Surface, *Ain Shams Eng. J.*, vol. **4**, no. 4, pp. 933-938, 2013.

[19] Brinkman, H.C., A Calculation of Viscous Force Exerted by a Flowing Fluid on a Dense Swarm of Particles, *Appl. Sci. Res.*, vol. **A1**, pp. 27-34, 1947.

[20] Deo, S. and Maurya, D.K., Generalized Stream Function Solution of the Brinkman Equation in the Cylindrical Polar Coordinates, *Spec. Topics Rev. Porous Media*, vol. **10**, no. 5, pp. 421-428, 2019.

[21] Maurya, D.K. and Deo, S., Stream Function Solution of the Brinkman Equation in Parabolic Cylindrical Coordinates, *Int. J. Appl. Comput. Math.*, vol. **6**, no. 6, pp. 1-10, 2020.

[22] Deo, S., Maurya, D.K. and Filippov, A.N., Influence of Magnetic Field on Micropolar Fluid Flow in a Cylindrical Tube Enclosing an Impermeable Core Coated with Porous Layer, *Colloid J.*, vol. **82**, no. 6, pp. 649–660, 2020.

[23] Deo, S., Maurya, D.K. and Filippov, A.N., Effect of Magnetic Field on Hydrodynamic Permeability of Biporous Membrane Relative to Micropolar Liquid Flow, *Colloid J.*, vol. **83**, no. 6, pp. 662–675, 2021.

[24] Tiwari, A. and Deo, S., Pulsatile Flow in a Cylindrical Tube with Porous Walls: Applications to Blood Flow, *J. Porous Media*, vol. **16**, no. 4, pp. 335–340, 2013.

[25] Maurya, D.K., Deo, S. and Khanukaeva, D.Y., Analysis of Stokes Flow of Micropolar Fluid Through a Porous Cylinder, *Math. Meth. Appl. Sci.*, vol. **44**, no. 8, pp. 6647–6665, 2021.

[26] Deo, S. and Maurya, P.K., Micropolar Fluid Flow Through a Porous Cylinder Embedded in Another Unbounded Porous Medium, *J. Porous Media*, vol. **24**, no. 4, pp. 89-99, 2021.

[27] Maurya, D.K. and Deo, S., Effect of Magnetic Field on Newtonian Fluid Sandwiched Between non-Newtonian Fluids Through Porous Cylindrical Shells, *Spec. Topics Rev. Porous Media*, vol. **13**, no. 1, pp. 75-92, 2022.

[28] Shercliff, J.A., *A Textbook of Magnetohydrodynamics*, Pergamon Press, 1965.

[29] Kumaran, V., Tiruchirappalli and Ramanaiah, G., A Note on the Flow Over a Stretching Sheet, *Acta Mech.*, vol. **116**, pp. 229-233, 1996.

[30] Pop, I. and Na, T., A Note on MHD Flow Over a Stretching Permeable Surface, *Mech. Res. Comm.*, vol. **25**, no. 3, pp. 263-269, 1998.

[31] Bhattacharyya, K., Hayat, T. and Alsaedi, A., Analytic Solution for Magnetohydrodynamic Boundary Layer Flow of Casson Fluid Over a Stretching/Shrinking Sheet With Wall Mass Transfer, *Chin. Phys. B*, vol. **22**, no. 2, pp. 1-6, 2013.

[32] Deo, S. and Maurya, D.K., Investigation of MHD Effects on Micropolar–Newtonian Fluid Flow Through Composite Porous Channel, *Microfluid. Nanofluid.*, vol. **26**, no. 8, Article no. 64, 2022.

[33] Jaiswal, S., Das, S. and Aguilar, J.F.G., A New Approach to Solve the Fractional Order Linear/Non-linear Two-Dimensional Partial Differential Equation Using Legendre Collocation Technique, *Few-Body Syst.*, vol. **63**, Article no. 56, 2022.